One Health Advances

ARTICLE

Open Access

Visual colorimetric immunosensor for sensitive detection of 4-Chlorophenoxyacetic based on TMB^{2+}-mediated etching of Au NRs

Jinzhi Han[1†], Cheng Peng[2†], Jiayan Wen[1], Xueming Cao[1], Yu Wang[2], Jingnan Meng[3*] and Zhenlin Xu[1*]

Abstract

4-Chlorophenoxyacetic acid (4-CPA), a synthetic plant regulator, has been banned due to its cumulative toxicity to humans. However, unqualified sampling remains common in the market. To address the poor sensitivity of 4-CPA antibodies reported previously, a highly sensitive monoclonal antibody specific to 4-CPA was produced by redesigning and synthesizing a novel hapten in this study. Additionally, a visual colorimetric immunosensor based on TMB^{2+} mediated etching of gold nanorods (Au NRs) was developed. The Δλ of the localized surface plasmon resonance (LSPR) peak exhibited a linear dependence on the 4-CPA concentration in the range of 0.2–6.25 ng mL^{-1}, with a low limit of detection (LOD) of 0.2 ng mL^{-1}. Recovery tests (85.0% to 108%) and HPLC validation demonstrated the immunosensor's accuracy and precision. This visual colorimetric immunosensor illustrates significant potential for rapid detection of 4-CPA in biological environments.

Keywords 4-chlorophenoxyacetic, Colorimetric immunoassay, Gold nanorods

Introduction

The phenolic plant growth regulator 4-Chlorophenoxyacetic acid (4-CPA), which is frequently present in bean sprouts [1, 2], is used to promote cell division while preventing root cell growth. It works by encouraging biosynthesis and biotransformation in plants, which thickens the hypocotyls of bean sprouts, inhibits root sprouting, and speeds up cell division during bean sprout culture [1–3]. However, 4-CPA is cumulatively toxic to humans, and consuming too much of it can be harmful to health and damage organs like the kidneys and liver [4, 5]. Acute toxicity testing on mice had shown an oral LD_{50} of 794 mg kg^{-1}. Consequently, many organizations and countries have either outright prohibited the use of 4-CPA in plant growth or set maximum residue limits (MRLs) [6]. For instance, the residual limit of 4-CPA in bean sprouts is 0.02 mg kg^{-1} in Japan and 0.01 mg kg^{-1} in the United States. However, monitoring data showed that 4-CPA residue levels in bean sprouts continued to significantly exceed the allowable limits.

Currently, instrumental analytical techniques such as gas chromatography, surface-enhanced Raman spectroscopy, and high-performance liquid chromatography (HPLC) are the main tools used to analyze 4-CPA in food [6–9]. However, these methods are expensive, cumbersome, require trained personnel, and can not provide rapid and portable on-site screening. In contrast, due to the simplicity and visual detection, colorimetric immunosensors based on gold nanomaterials have been

[†]Jin-Zhi Han and Cheng Peng these authors contributed equally to this work.

*Correspondence:
Jingnan Meng
xuanwangmjn@163.com
Zhenlin Xu
jallent@163.com
[1]Guangdong Provincial Key Laboratory of Food Quality and Safety, South China Agricultural University, Guangzhou 510642, China
[2]Guangzhou Institute of Food Inspection, Guangzhou 510410, China
[3]College of Food Engineering, Anhui Science and Technology University, Chuzhou 233100, China

considered one of the most promising immunoassay methods in recent years [10–13]. For instance, Hu et al. [14] designed a colorimetric sandwich immunosensor for Aβ based on dual antibody-modified gold nanoparticles, in which maintaining the excellent performance of ELISA while improving visualization and sensitivity to 2.3 nM due to the introduing of gold nanoparticles. Gold nanomaterials used in such immunoassays are mainly of the following three types: gold nanoclusters, gold nanoparticles, and gold nanorods. Gold nanorods are the most widely used in therapeutic, detection and other fields [15–17].

The colorimetric sensors based on gold nanorods take advantage of the strong localized plasmon resonance effect of gold nanorods [18]. Au NRs have two localized surface plasmon resonance (LSPR) peaks, corresponding to the transverse and longitudinal peaks, respectively. These peaks are highly sensitive to the size, shape and composition of Au NRs, especially the longitudinal LSPR peak, which located in the visible to near-infrared range [17]. By exploiting the adjustable property of longitudinal LSPR peaks, there have aroused extensive interest in the field of semi-quantitative detection of nucleic acids, proteins and small molecules with the naked eye. For example, Zhu et al. [19] successfully developed a nanosensor based on gold nanorods for the sensitive and selective quantitative detection of antibiotic residues, which was simple, rapid, inexpensive, and able to monitor antibiotics at concentrations below 0.1 ng mL^{-1} in less than 2 h.

In this study, the new hapten structures were designed and synthesized, and artificial antigens were prepared by conjugating them with carrier proteins. Monoclonal antibodies (mAbs) that specifically recognize 4-CPA were generated through techniques such as animal immunization and hybridoma cell screening. Building on the mAbs, a visual colorimetric immunoassay based on Au NRs was developed and applied to real samples detection. The simplicity and sensitivity of the analysis were significantly enhanced by utilizing enzyme-labeled immunoreaction in conjunction with the color shift caused TMB^{2+} etching Au NRs. This approach has the potential for sensitive visual identification in complex food testing for market field screening.

Results and discussion

Identification of hapten and artificial antigen

The molecular structure of 4-CPA contains carboxyl active groups that can directly interact with proteins. To maintain the integrity of the 4-CPA molecule and enhance antibody specificity, a complete synthesis scheme was proposed. A spacer arm comprising 5 to 6 carbon chains were connected to the benzene ring of 4-CPA. This design will ensure that the hapten's small molecule is fully accessible on the surface of the artificial antigen, maximizing immune system recognition while preserving the carboxyl group in the structure of 4-CPA through coupling with the epoxy group. In order to confirm the successful synthesis of the hapten, the synthesized hapten was separated, purified using thin layer chromatography, and then it was structurally characterized using mass spectrometry employing either ESI negative or positive ions. Fig. S1 demonstrated that the mass spectrum of 4-CPA-H1 has a molecular peak of 269, and the positive or negative ion spectrum profiles matched the molecular weight of the target hapten. Furthermore, the split peaks in the hydrogen ion spectrum of NMR (Fig. S2) confirmed the correct synthesis of the hapten.

Comparing the UV-vis spectra of the hapten, carrier protein, and final binding protein, the absorbance peaks in Fig. 1A were significantly shifted, indicating that the artificial antigen 4-CPA-H1-BSA ans 4-CPA-H1-OVA were successfully prepared.

Characterization of mAbs

In this work, 4-CPA was directly coupled with BSA to yield an immunogen and with OVA to yield a coating antigen. After mice immunization and cytochemical fusion, a hybridoma cell line (4-A7) was obtained that secreted mAbs against 4-CPA. After purification by affinity column chromatography using ProteinA/G as medium, the mAbs demonstrated high purity (Fig. 1B), and the isotype was identified as IgG1 (Fig. 1C). In addition, the half-maximal inhibitory concentration (IC_{50}) was 0.8 ng mL^{-1} under the optimal ELISA conditions (Fig. 1D) after optimizing the pertinent icELISA parameters in this research (results were showed in Fig. S3 and Fig. S4). Moreover, the specificity of mAbs was evaluated through the structural analogues' cross-reactivity (CR % = IC_{50} (4-CPA)/ IC_{50} (structural analogues) × 100). The negligible CR indicated that the mAbs had good specificity and were feasible for analytical detection (Table 1).

Characterization of Au NRs

The two steps of synthesis process utilized in this work were the synthesis of gold seeds and the growth of gold rods, respectively. The synthesis process was mediated by anion-assisted seeds. The color of a typical seed solution was a tea-brown, whereas the generated Au NRs were a purplish red hue (Fig. S5). TEM was used to examine the Au NRs for microscopic morphology [20] after the Au NRs solution was etched in different concentrations of TMB^{2+} for a predetermined amount time (Fig. 2). Figure 2A–H sequentially represent the gradual increase in the concentration of TMB^{2+} solution. It was observed that the aspect ratio of Au NRs decreased with increasing TMB^{2+}

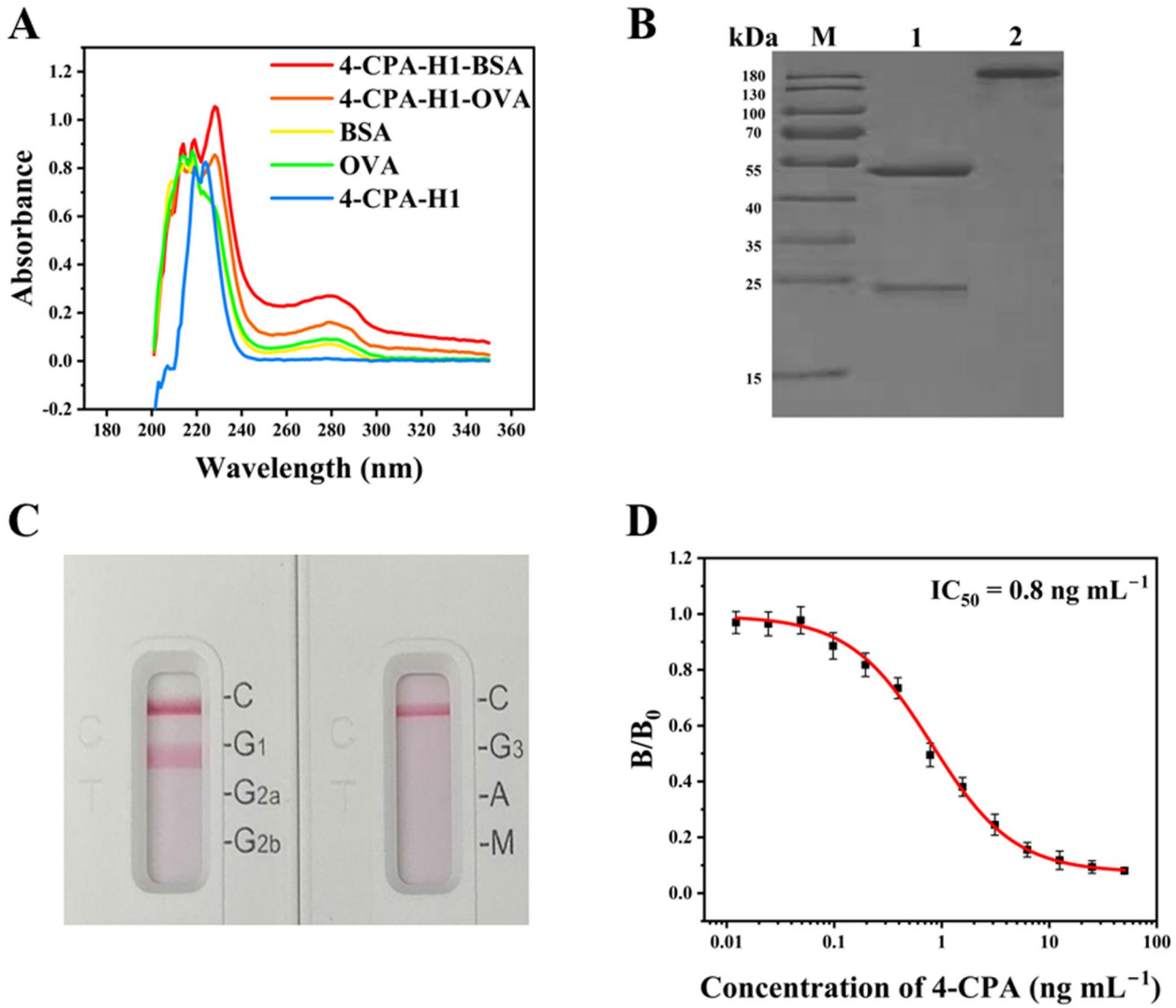

Fig. 1 Characterization of mAbs against 4-CPA. **A** The UV–vis spectra of the protein, hapten, and artificial antigen. **B** Purity identification of mAbs, M: marker, 1: reducing gel, 2: non-reducing gel. **C** Isotype of mAbs. **D** Sensitivity of mAbs using indirect competitive ELISA (icELISA)

concentration. Specifically, the longitudinal LSPR of Au NRs was 730 nm, with a mean value of the length of 64 nm, and the aspect ratio of 4.2 (Fig. 2A). At 705 nm, the ends of Au NRs were gradually etched to become rounded, with the mean value of the length of 59 nm, and the aspect ratio of 3.6 (Fig. 2B). At 680 nm, both ends of the Au NRs were gradually shortened by etching, with an average length value of 55 nm and a transverse-to-vertical ratio of 3.1 (Fig. 2C). Further etching reduced the longitudinal LSPR to 660 nm, with an average length value of 43 nm and a transverse-to-vertical ratio of 2.6 (Fig. 2D). At 640 nm, the Au NRs had an average length of 35 nm and a transverse-to-vertical ratio of 2.2 (Fig. 2E). Finally, at 620 nm, with a mean value of the length of 24 nm, and the transverse to longitudinal ratio is 1.7 (Fig. 2F). The gold nanoparticles were etched into gold nanoparticles tending to be rounded shapes, from long rods at right angles to long rods with both ends rounded gradually, and then from long rods to short rods. It was evident that as the length of the Au NRs gradually decreases, the transverse to longitudinal ratio decreases. Figure 3A–H correspond respectively to the colors and UV–vis absorption spectra of the Au NRs in Fig. 2A–H at different etching levels. As the longitudinal LSPR peaks of Au NRs are continuously blue-shifted, a series of color changes including red, grey, lime green, blue, blue-violet, violet and pink occur (Fig. 3A–H). The solution turned yellow when Au NRs were fully etched to Au (I). Equation (1) provided the specific mechanism.

Table 1 The cross-reactivity with structural analogues using icELISA

Analytes	Structure	IC_{50} (ng mL^{-1})	CR (%)
4-CPA	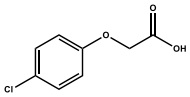	0.8	100
2,4-Dichlorophenoxyacetic acid	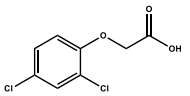	2.5	32
4-Formylphenoxyacetic acid	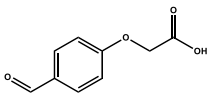	5.2	15.4
Phenoxyacetic acid	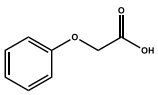	50.1	1.6
4-Aminophenoxyacetic acid	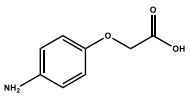	74.9	1.1
4-Chlorobenzoic acid	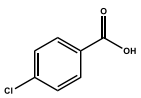	> 1000	< 1
4-Chlorophenylacetic acid	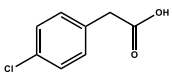	> 1000	< 1
6-Benzyladenine	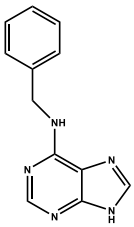	> 1000	< 1

$$\mathrm{TMB(II)} + 2\mathrm{Au} = \mathrm{TMB} + 2\mathrm{Au(I)} \quad (1)$$

Feasibility of multicolor immunoassay based TMB etched gold nanorods

Alterations in TMB^{2+} concentration can lead to changes in Au NRs morphology. To construct a visual colorimetric immunosensor, this work also verifies the feasibility of TMB^{2+} effectively etching the Au NRs, resulting in changes in the morphology of the gold nanoparticles and the color of the solution. The color and UV–visible spectra plots of different solutions were shown in Fig. S6. The Au NRs solution is red with a UV absorption spectrum peak at approximately 730 nm; the TMB^{2+} solution is yellow with a UV absorption spectrum peak at around 450 nm; and the Au NRs + TMB^{2+} solution is green with UV absorption spectrum peaks at 450 nm and 730 nm, indicating that the two coexist without reacting. However, the solution of Au NRs + CTAB + TMB^{2+} showed a light purple color, and the UV absorption peak was blue-shifted, demonstrating that the Au NRs were successfully etched. This suggests that the presence of cationic surfactant, such as CTAB, is necessary for the successful etching of Au NRs by TMB^{2+}.

Optimization of multicolor immunoassay conditions

From the above, it was evident that the color change of Au NRs was caused by TMB^{2+} etching. In the traditional ELISA process, the concentration of horseradish peroxidase (HRP), H_2O_2, and TMB can affect TMB^{2+} generation [21]. Hence, the concentrations of HRP, H_2O_2 and TMB were first evaluated.

The sensor's absorption peak wavelength shift ($\Delta\lambda$) gradually increased as the concentration of H_2O_2 increased, reaching its maximum value when H_2O_2 was 4 mM (Fig. 4A), and then the value of $\Delta\lambda$ stabilized at around 200 nm. Since hydrogen peroxide is the catalytic substrate of the HRP enzyme, excessive hydrogen peroxide inhibits the enzyme activity, and the optimal concentration was 4 mM. Likewise, the $\Delta\lambda$ gradually increased with the increase of TMB concentration, reaching its maximum value when the concentration of TMB was 4 mM (Fig. 4B). When the concentration of TMB increased to 5 mM, $\Delta\lambda$ no longer increased. Although TMB is stable, its solubility is low, and overdosing can lead to precipitation in the system, so the optimal concentration was set at 4 mM. As the HRP dilution decreased, $\Delta\lambda$ gradually increased, reaching its maximum value at a dilution of 2 K (Fig. 4C).

It is worth mentioning that, according to electrochemical thermodynamics, the reaction potential of TMB^{2+}/TMB is 0.74 V [22], which is lower than that of Au(I)/Au at 0.91 V [23]. This indicates that CTAB reduces the reaction potential, making it essential for the etching process. Therefore, the concentration of CTAB was optimized, and $\Delta\lambda$ gradually increased with the increase of CTAB concentration, reaching its maximum value when the concentration of CTAB was 0.1 M (Fig. 4D). In conclusion, the optimal HRP dilution for the 4-CPA colorimetric immunosensor was 2 K, the optimal concentration of CTAB was 0.1 M, and the concentrations of H_2O_2 and TMB were both 4 mM.

The performance of colorimetric immunosensor

The colorimetric immunosensor was developed based on the above optimal reaction conditions. In the range of 0 to 25 ng mL^{-1}, the standard curve (Fig. 5A) was established with the 4-CPA concentration as the horizontal coordinate and the maximum absorption peak wavelength shift as the vertical coordinate. As the concentration of 4-CPA decreased, the etching degree of gold nanorods gradually strengthened, the longitudinal

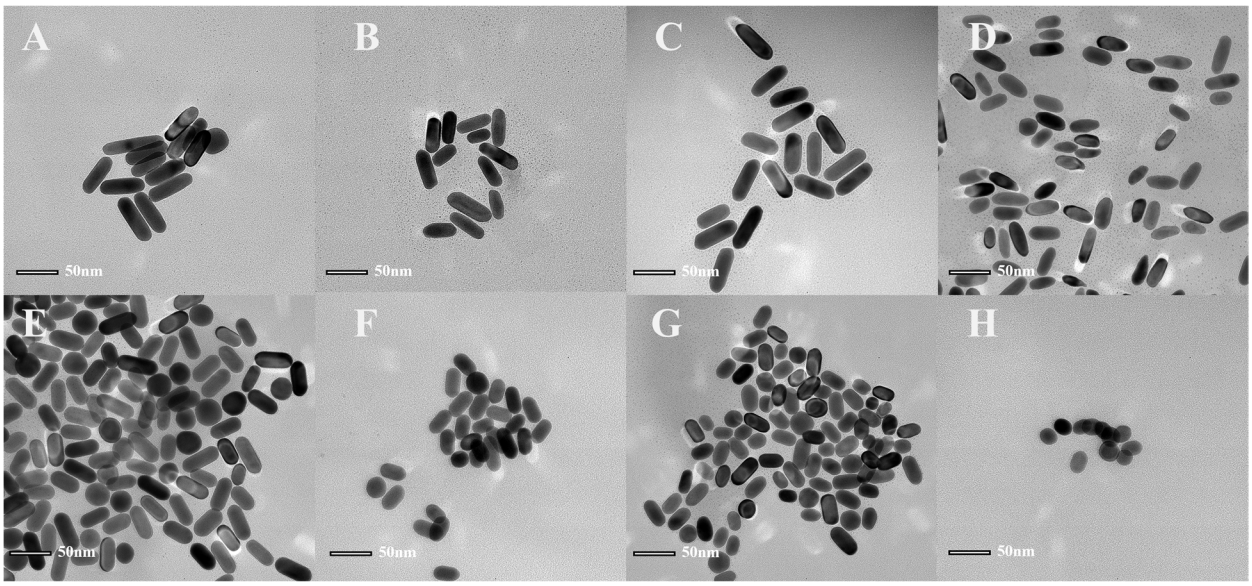

Fig. 2 TMB^{2+} induced etching of Au NRs. **A–H** TEM images of as-prepared Au NRs at different magnifications after etching

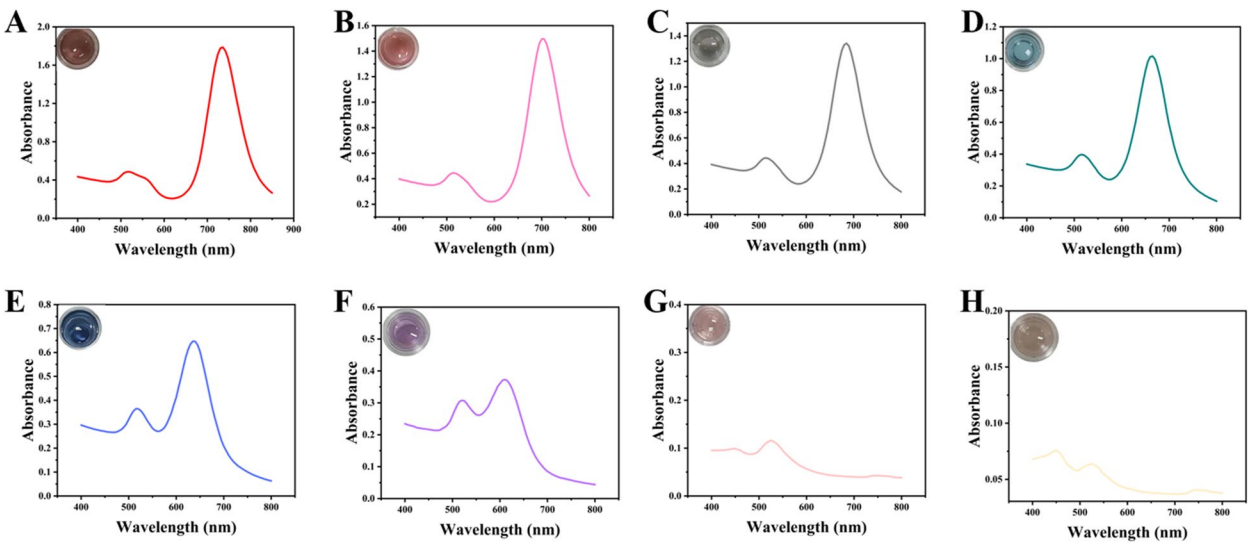

Fig. 3 The photographs of AuNRs with different levels of etching and corresponding UV-vis absorption spectra (A–H)

direction of the LSPR peak was shifted to shorter wavelengths (Fig. 5B), and the system exhibited a series of color changes from red, grey, lime green, blue, blue-violet, violet to pink (Fig. 5C). Remarkably, this vivid color significantly enhances the colorimetric system's resolution for the naked-eye detection. In the meantime, the longitudinal peak shift of the LSPR showed a linear relationship with the 4-CPA concentration in the range of 0.2–6.25 ng mL^{-1} as the Au NRs were continuously etched. The standard curve was $\Delta\lambda = -62.11\ C_{4\text{-CPA}} + 68.37$ ($R^2 = 0.993$), with a detection range of 0.2–6.25 ng mL^{-1} and the limit of detection of 0.2 ng mL^{-1}, calculated from the standard curve equation: the concentration of 4-CPA corresponding to 10% inhibition was used as the limit of detection. The high sensitivity of the colorimetric immunosensor provides significant advantages in the field detection. The specificity of this immunosensor relies on the specificity of the mAbs, and the cross-reactivity rate in Table 1 serves as compelling evidence of the sensor's high specificity. To evaluate the accuracy and precision of the colorimetric immunosensor, the linear ranges of the standard curves

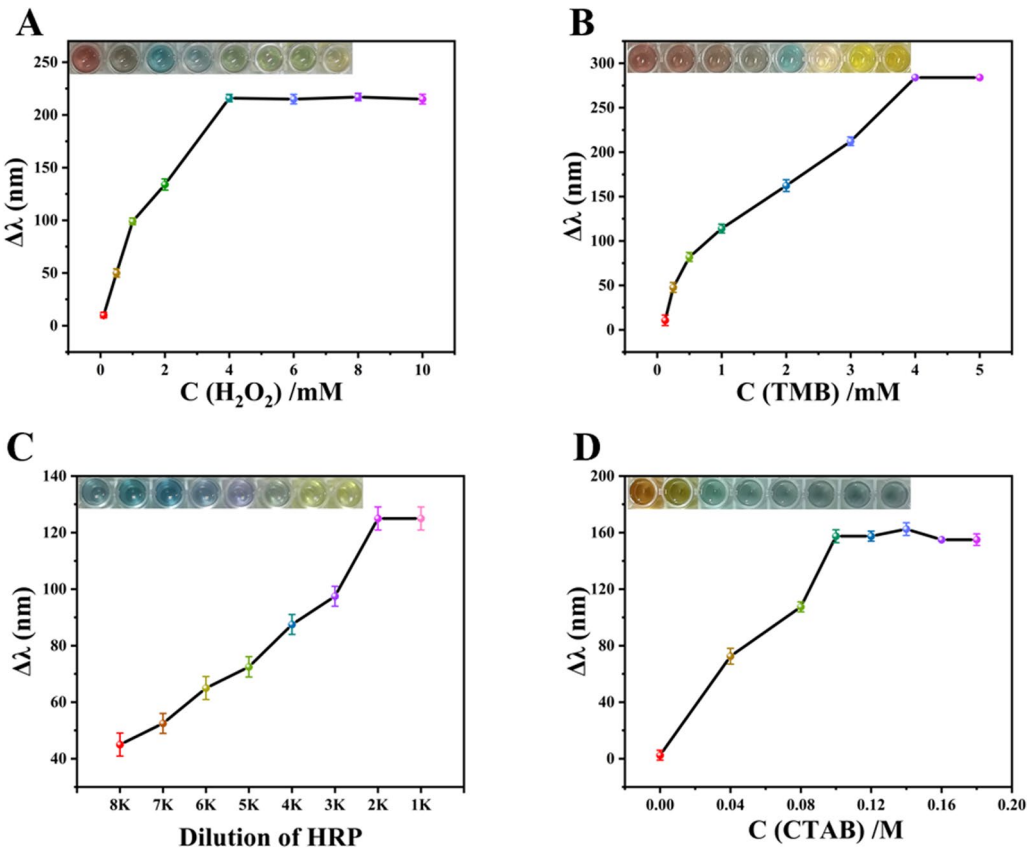

Fig. 4 Optimization of the process of etching. **A** The concentration of H_2O_2. **B** The concentration of TMB. **C** The dilution of HRP. **D** The concentration of CTAB

for various samples were used as the reference basis, and three standard solutions of 4-CPA with known concentrations (high, medium and low) were added to average spiked recoveries and coefficients of variation were calculated. The amounts of standard solutions were spiked at 0, 80, 280, and 1060 μg kg^{-1}, respectively. The results are shown in Table 2. The recoveries ranged from 85% to 108%, and the relative standard deviations (RSDs) were in the range of 4.3%–9.8% ($n=3$). Other methods for the detection of 4-CPA are listed in Table S2 for comparison. These results indicate that the immunosensor is highly reliable and reproducible.

To explore the reproducibility and stability of this colorimetric immunosensor, five sets of sensors were constructed simultaneously to detect 4-CPA (2 ng mL^{-1}) under the same conditions, assessing both intra-group and inter-group reproducibility. The data is presented in the Fig.S7 A and Fig.S7 B, with the coefficient of variation at 1.47% and 4.25%. Additionally, daily UV–visible spectral scans were recorded using a microplate reader. As shown in Fig. S7 C, Δλ remained at about 70% of the initial response. These results indicate that the sensor has good reproducibility and stability.

In addition, the method's accuracy was verified by comparing the results with HPLC data shown in Table 2. A strong correlation between the colorimetric immunoassay and the HPLC results was observed, indicating that the colorimetric immunosensor is both reliable and promising for real sample detection.

Conclusion

In this study, to address the current issue of poor sensitivity of 4-CPA mAbs, a total synthesis scheme was designed to ensure the hapten was fully exposed on the surface of the artificial antigen. And later, based on the mechanism of antigen–antibody specific reaction, a highly sensitive mAbs specifically recognizing 4-CPA was successfully prepared, which reached the detection range of 0.24–2.73 ng mL^{-1}, with the detection limit of 0.12 ng mL^{-1}, and the sensitivity was up to 0.8 ng mL^{-1} in ELISA. The acquired antibody was then efficiently used to develop a visual colorimetric immunosensor with Au NRs as the chromogenic substrate. The sensor exhibited high sensitivity (LOD = 0.2 ng mL^{-1}) and demonstrated high accuracy in real sample detection, showing excellent agreement with the results of HPLC. Moreover, since

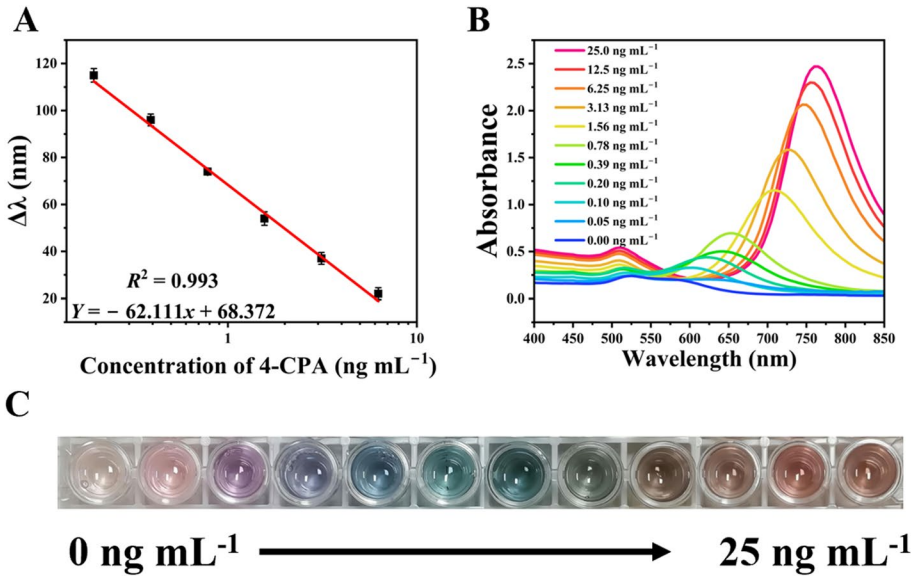

Fig. 5 The performance of dual-modular immunosensor. **A** Plotting of Δλ versus 4-CPA concentrations. **B** Plotting of UV–Vis spectral scans. **C** Photographs of the immunosensor at different concentrations of 4-CPA (0–25 ng mL^{-1})

etching of Au NRs results in a color change, rapid semi-quantitative detection can be performed by visual observation or via smartphone photography. This capability highlights its potential for on-site detection of complex food products. Therefore, the immunosensor developed in this study can be readily used for rapid screening of illegally added 4-CPA in vegetables, thereby contributing to reducing the incidence of foodborne illnesses and improving food safety.

Materials and methods

Materials and reagents

4-Chlorophenoxyacetic acid (4-CPA), chloroauric acid ($HAuCl_4$) for the synthesis of Au NRs were purchased from Sinopharm Chemical Reagent Co., Ltd (Shanghai, China). Bovine serum albumin (BSA), ovalbumin (OVA), keyhole limpet hemocyanin (KLH), N-Hydroxysuccinimide (NHS) and 3-dimethylaminopropyl were purchased from Sigma-Aldrich (St. Louis, MO, USA). Microporous

Table 2 Recoveries of spiked samples by colorimetric immunosensor and HPLC ($n = 3$)

Sample	Spiked level	visual image	Colorimetric Immunosensor					HPLC
	μg kg^{-1}	Figure	Mean μg kg^{-1}	Recovery%	RSD %	Mean μg kg^{-1}	Recovery %	RSD %
Soy bean sprouts	0		ND	–	–	ND	–	–
	80		72	90 ± 5.9	6.5	93	116 ± 5.2	4.5
	280		264	94 ± 5.1	5.4	300	107 ± 6.4	6.0
	1060		1140	108 ± 10.6	9.8	993	94 ± 1.5	1.6
Mung bean sprouts	0		ND	–	–	ND	–	–
	80		68	85 ± 4	4.7	82	103 ± 2.3	2.2
	280		247	88 ± 3.8	4.3	321	115 ± 5.8	5.0
	1060		991	94 ± 6.8	7.2	1103	104 ± 3.3	3.2

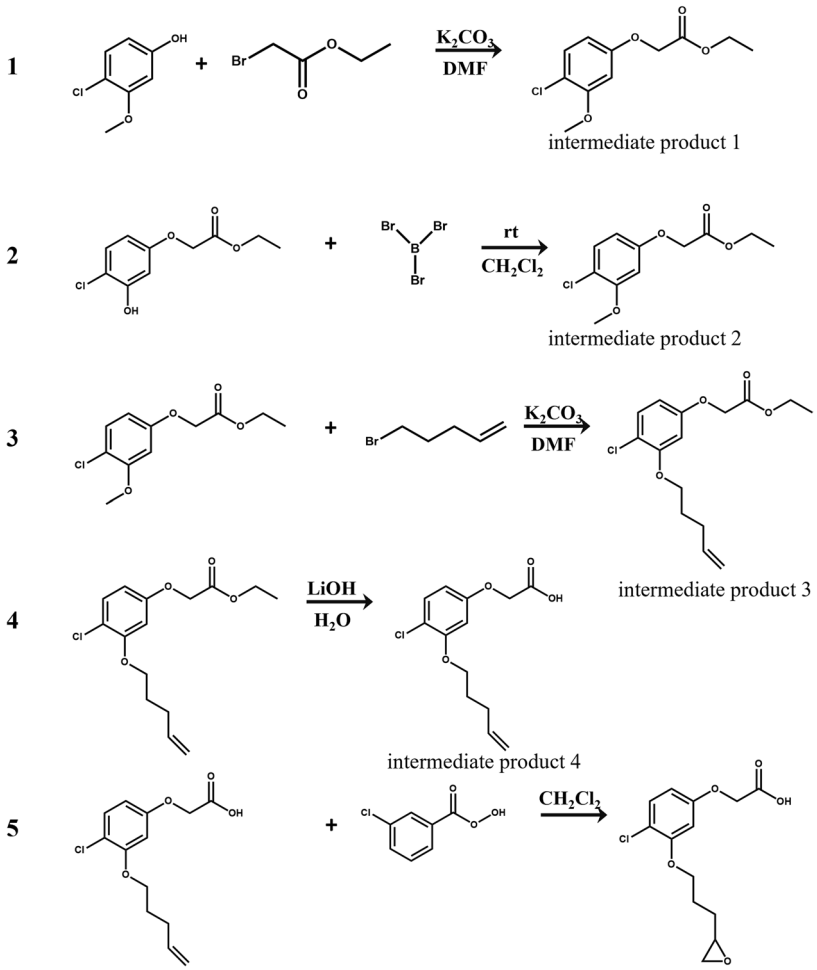

Fig. 6 Synthetic route for the hapten 4-CPA-H1

filters (0.22 μm) were purchased from Jinteng experimental equipment Co., Ltd (Tianjin, China). Balb/c female mice were purchased from Beijing Vital River Laboratory Animal Technology Co., Ltd (Beijing, China) and raised at the Animal Experiment Centre of South China Agriculture University (Animal Experiment Ethical Approval Number: 2021B050). All chemicals and reagents were of analytical grade.

Instruments

The SpectraMax i3x multifunction measuring instrument for absorption spectra measurement was purchased from Molecular Devices (Sunnyvale, CA, USA). Nanodrop 2000C system for quantifying the concentration of proteins, Talos G2200X electronic microscope for obtaining the transmission electron microscopy (TEM) images, and the microplate reader for absorbance measurement were purchased from Thermo Fisher Scientific (Waltham, MA, USA). Milli-Q Ultrapure Water System was purchased from Milli-Q Millipore (Bedford, MA, USA). The mass spectrometer (QP_{50}) for analytical comparisons was purchased from Shimaduze (Shimadzu, Japan).

Preparation of hapten and artificial antigen

The synthetic route for the hapten 4-CPA-H1 is shown in Fig. 6. The steps are as follows: 4-chloro-3-methoxyphenol (0.5 g, 3.15 mM) and methyl bromoacetate (0.725 g, 4.73 mM) were dissolved in 5 mL of DMF and K_2CO_3 (1.5 g, 12.6 mM) was added for reaction for 4 h at 110 °C. The reactants were extracted three times repeatedly by adding 50 mL of water and 20 mL of ethyl acetate. The ethyl acetate was removed by evaporating. Then the intermediate product 1 was obtained. For the next step, a 100 mL double-necked round-bottomed flask was dried in an oven at 98 °C for 2 h. After evaporation, 5 mL of anhydrous CH_2Cl_2 was added to flask to dissolve intermediate product 1, then 1 mL of BBr_3 was slowly added under low-speed stirring and the mixture reacted overnight at a low temperature. After the reaction was completed, the methanol was added drop by drop to quench

the BBr_3. The solution was extracted and the organic layer was evaporated to obtain the intermediate product 2. In the third step, the intermediate product 2, 5-bromo-1-pentene (0.9 g, 6.3 mM), and K_2CO_3 (1.3 g, 9.45 mM) were dissolved in 5 mL of DMF solution and reacted at 110 ℃ under the condition of 4 h. After the reaction, the extraction was added to 50 mL of water and 20 mL of ethyl acetate to extract 3 times, the organic layer was evaporated to obtain intermediate product 3. The intermediate product 3 was dissolved in 2 mL of methanol and 0.4 g of lithium hydroxide and 10 mL of water were added at 70 °C for 2 h. Then the organic layer was evaporated, the residual solution was purified by column to obtain intermediate 4. The intermediate 4 was dissolved in 5 mL of CH_2Cl_2 and reacted with m-chloroperoxybenzoic acid (0.82 g, 4.73 mM) at room temperature for 4 h. The reaction product was purified by column chromatography and the final product was obtained.

The procedure for synthesis of artificial antigens is as follows: Firstly, 0.091 g of hapten (4-CPA-H1) was dissolved in 50 μL of DMF. And 20 mg of BSA or OVA was dissolved in 20 mL of CB buffer (pH 9.6) at a concentration of 1 mg mL^{-1}. The above DMF solution was added dropwise with stirring, and the pH of the solution was measured after the dropwise addition. If the pH was low, sodium hydroxide solution was added dropwise to adjust the pH of the mixture to 8 ~ 9. The solution was then dialyzed in PBS (0.01 M, 5.0 L) for 3 days to obtain the conjugation mixture and then stored at −20 °C.

Production of mAbs

Balb/c female mice (8–9 weeks) were immunized with the immunogen (4-CPA-BSA) according to the immunization scheme (Table S1). The immunization cycle was conducted fortnightly. Freund's complete adjuvant was used for the first immunization and Freund's incomplete adjuvant was used for booster immunization [24]. The method of injection was multipoint subcutaneous. Hybridoma cells were formed by fusing mouse spleen cells, which had the best titer, with $SP_{2/0}$ myeloma cells using a polyethylene glycol (PEG) fusion promoter. Subsequently, cells with better titer were subcloned five times using limited dilution. The monoclonal cell line with the best results was gained and finally mAbs were obtained by purifying ascites.

Synthesis of Au NRs

The synthesis of gold seeds and the growth of gold rods are the two steps of synthesis process utilized in this study [25], which is mediated by silver ion-assisted seeds [26]. Briefly, freshly prepared ice-cold $NaBH_4$ solution was added to a 15 mL glass tube containing $HAuCl_4$ and CTAB under vigorous stirring. The seed solution had a color change from yellow to brownish yellow following two minutes of vigorous stirring at 1200 rpm. Before use, the seed solution was allowed to kept at room temperature for at least 30 min after the stirring was ceased.

Preparation of growth solutions: CTAB (50 mL, 0.2 M) and sodium oleate solids (0.2476 g) were fully dissolved in 50 mL of ultra-pure water. Ascorbic acid (5.5 mL, 0.1 M) was added to a well mixed solution containing $HAuCl_4$ (5 mL, 0.01 M) and $AgNO_3$ (0.6 mL, 0.01 M). The mixture solution was diluted to 50 mL with ultrapure water. After through mixing and stirring for 30 min, the color of the solution gradually faded from yellow to nearly colorless.

Finally, 200 μL of seed solution was injected into the growth solution. The mixture was stirred vigorously and allowed to stand at 30 °C for 24 h. To remove the supernatant, the synthesized Au NRs were centrifuged at 11,000 rpm for 15 min. The precipitate was then redispersed into the same volume of CTAB solution and the above procedure was repeated twice.

Fabrication of visual colorimetric immunosensor for 4-CPA detection

Au NRs can react with TMB^{2+} to form TMB^{+} while Au is oxidized to Au(I). This oxidation process selectively occurs at the ends of the Au NRs, resulting in the shortening of the Au NRs while keeping the transverse diameter almost unchanged [27]. Based on this property, the colorimetric sensor developed in this study uses the TMB^{2+} generated during the conventional icELISA reaction to etch the Au NRs [28], causing a series of color changes as polychromatic optical signals.

Before constructing the colorimetric immunosensor, the optimal dilution concentrations of the coated antigen and antibody were determined using the checkerboard method, and the type of reaction buffer and the ionic concentration were optimized in this study (experimental parameters are provided in Supporting information). Under the optimized experimental conditions, the colorimetric immunosensor procedure was as follows: Firstly, a 96-microwell plate was coated with 100 μL of 4-CPA-H1-OVA (1 μg mL^{-1}) and incubated for a 12 h at 37 °C. After that, the plate was then rinsed twice with 0.1 M PBST (PBS containing 0.5% Tween 20), blocked with 3% bovine albumin in 0.1 M PBS (200 μL $well^{-1}$) at 37 °C for 2 h, and dried at 37 °C for 30 min. Later, 50 μL of 4-CPA (at various concentrations in PBS) was added to each well, followed by adding 50 μL of mAbs in PBS. After incubation for 40 min at 37 °C, the wells were washed with PBST five times. Subsequently, 100 μL of HRP-Sheep anti-mouse IgG (secondary antibody) (1:5000 in PBST) was injected and incubated for 30 min, and the plate was rewashed

five times to remove the unconjugated secondary antibody. Then, 100 μL of color development substrate (containing TMB and H_2O_2) was added to each well and incubated at 37 ℃ for 10 min. Followed by adding 2 M H_2SO_4 solution (50 μL) for 10 min, 80 μL of Au NRs solution was pipetted into each well and incubated for 15 min at 37 °C. Finally, the UV–vis spectrum ranging from 400 to 800 nm and color of the solution were measured with a microplate reader and a smartphone, respectively. The immunosensor standard curve was generated by plotting the LSPR blue-shifted value of Au NRs ($\Delta\lambda$, $\Delta\lambda = \lambda_{max} - \lambda$, λ_{max} denotes the wavelength value without 4-CPA, and λ denotes wavelength value at the maximum concentration of 4-CPA) versus the 4-CPA concentration. The assay's LOD was determined as IC_{10} with the lower and upper limits of quantitative concentration as IC_{20} and IC_{80}, respectively.

Detection of real samples

The accuracy and precision of colorimetric immunosensor were evaluated by spiking real samples with different concentrations of 4-CPA standards to determine the recovery, compared with the results of HPLC analyses. Four concentrations of 4-CPA (0, 80, 280, 1060 μg mL^{-1}) were spiked into negative samples (soybean sprouts and mung bean sprouts), and three parallel of each spiked concentration were set up. All extracts were diluted 20-fold to eliminate the matrix effect.

Supplementary Information

The online version contains supplementary material available at https://doi.org/10.1186/s44280-024-00062-y.

Supplementary Material 1.

Acknowledgements
This work was supported by the National Key Research and Development Program of China (2023YFF1105002) and the Key Project of Guangdong Provincial High School, China (2022ZDZX2004).

Authors' contributions
J.H. and C.P. performed all experiments; J.W. and X.C. analyzed the data and prepared all figures; Y.W., J.M. and Z.X. wrote the manuscript. All authors read and approved the final manuscript.

Data availability
All data generated or analyzed during this study are included in its supplementary information files.

Declarations

Ethics approval and consent to participate
In the present study, all animal experiments were conducted in accordance with the protective and administrative laws for laboratory animals in China and were approved by the Institutional Authority for Laboratory Animal Care at South China Agricultural University, Guangzhou, China (Animal Experiment Ethical Approval Number: 2021B050).

Consent for publication
The data in this manuscript have not been previously reported by the authors or considered for publication elsewhere. All authors participated, reviewed and approved the final submitted version of the manuscript.

Competing interests
All authors declare no conflict of interest.

Received: 27 May 2024 Revised: 14 August 2024 Accepted: 28 September 2024
Published online: 31 October 2024

References

1. Ji SL, Qi L, Li N, Wang ML. Preparation of amino acid-based polymer functionalized magnetic nanoparticles as adsorbents for analysis of plant growth regulators in bean sprouts. Talanta. 2016;158:229–34.
2. Han YH, Yang CL, Zhou Y, Han DD, Yan HY. Ionic liquid-hybrid molecularly imprinted material-filter solid-phase extraction coupled with HPLC for determination of 6-Benzyladenine and 4-Chlorophenoxyacetic Acid in bean sprouts. J Agric Food Chem. 2017;65(8):1750–7.
3. Long L, Liang JJ, Zhu X, Xiao K, Li TZ, Hu JF. Auxin- and cytokinin-induced berries set in grapevine partly rely on enhanced gibberellin biosynthesis. Tree Genet Genomes. 2016;12:41.
4. Chuang JC, Emon JMV, Durnford J, Thomas K. Development and evaluation of an enzyme-linked immunosorbent assay (ELISA) method for the measurement of 2,4-dichlorophenoxyacetic acid in human urine. Talanta. 2005;67(3):658–66.
5. Kaya B, Yanikoglu A, Marcos R. Genotoxicity studies on the phenoxyacetates 2,4-D and 4-CPA in the drosophila wing spot test. Teratog Carcinog Mutagen. 1999;19(4):305–12.
6. Qin GF, Zou KT, Tian L, Li YB. Determination of five plant growth regulator containing carboxyl in bean sprouts based on chemical derivatization by GC-MS. Food Anal Methods. 2018;11(9):2628–35.
7. Shin E, Choi J, Abd El-Aty AM, Khay S, Kim S, Im M, et al. Simultaneous determination of three acidic herbicide residues in food crops using HPLC and confirmation via LC-MS/MS. Biomed Chromatogr. 2011;25(1–2):124–35.
8. Dobrev PI, Havlíček L, Vágner M, Malbeck J, Kamínek M. Purification and determination of plant hormones auxin and abscisic acid using solid phase extraction and two-dimensional high performance liquid chromatography. J Chromatogr A. 2005;1075(1–2):159–66.
9. Cai C, Yao F, Li C, Xiang YN, Wu PG, Hu ZY, et al. Determination of ten plant growth regulators in bean sprouts by mixed solid phase extraction columns separation and LC-MS/MS. Processes. 2023;11(9):2586.
10. Shen CM, Wang L, Zhang HY, Liu SJ, Jiang JW. An electrochemical sandwich immunosensor based on signal amplification technique for the determination of alpha-fetoprotein. Front Chem. 2020;16(8): 589560.
11. Chu BY, Qi TT, Liao JF, Peng JR, Li WT, Fu SZ, et al. Colorimetric detection of cancer biomarker based on pH induced color change. Sens Actuators B Chem. 2012;166–167:56–60.
12. Zhou YF, Huang XL, Zhang WJ, Ji YW, Chen R, Xiong YH. Multibranched gold nanoflower-embedded iron porphyrin for colorimetric immunosensor. Biosens Bioelectron. 2018;102:9–16.
13. Verdoodt N, Basso CR, Rossi BF, Pedrosa VA. Development of a rapid and sensitive immunosensor for the detection of bacteria. Food Chem. 2017;221:1792–6.
14. Hu T, Lu SS, Chen CX, Sun J, Yang XR. Colorimetric sandwich immunosensor for $A\beta_{(1-42)}$ based on dual antibody-modified gold nanoparticles. Sens Actuators B Chem. 2017;243:792–9.
15. Lebepe TC, Parani S, Maluleke R, Ncapayi V, Aladesuyi OA, Komiya A, et al. NIR-II window absorbing graphene oxide-coated gold nanorods and graphene quantum dot-coupled gold nanorods for photothermal cancer therapy. Nanotechnology reviews (Berlin). 2023;12(1):1891–907.
16. Sun QM, Shi XL, Feng JT, Zhang Q, Zhuo A, Ji YA, et al. Cytotoxicity and cellular responses of gold nanorods to smooth muscle cells dependent on surface chemistry coupled action. Small. 2018;14(52):1803715.
17. Eltai NO, Mahmoud NN, Zakaria ZZ, Abdelrahman H, Moustafa A, Al-Asmakh M. Antibacterial and antibiofilm activity of mercaptophenol functionalized-gold nanorods against a clinical isolate of

methicillin-resistant *Staphylococcus aureus*. J Inorg Organomet Polym Mater. 2022;32(7):2527–37.
18. Zheng JP, Cheng XZ, Zhang H, Bai XP, Ai RQ, Shao L, et al. Gold nanorods: the most versatile plasmonic nanoparticles. Chem Rev. 2021;121(21):13342–453.
19. Zhu HS, Liu CH, Liu XX, Zhu Q, Liu WP, Liu YJ. A multi-colorimetric immunosensor for visual detection of ochratoxin A by mimetic enzyme etching of gold nanobipyramids. Microchim Acta. 2021;188:62.
20. Kim H, Murata MM, Chang H, Lee SH, Kim J, Lee JH, et al. Optical and electron microscopy for analysis of nanomaterials. In: Jun B, editor. Nanotechnology for bioapplications. Singapore: Springer Nature; 2021. p. 277–287.
21. Liang CZ, Jin RY, Gui WJ, Zhu GN. Enzyme-linked immunosorbent assay based on a monoclonal antibody for the detection of the insecticide triazophos: assay optimization and application to environmental samples. Environ Sci Technol. 2007;41(19):6783–8.
22. Cao FH, Kim J, Bard AJ. Detection of the short-lived cation radical intermediate in the electrochemical oxidation of N, N-Dimethylaniline by scanning electrochemical microscopy. J Am Chem Soc. 2014;136(52):18163–9.
23. Rodríguez-Fernández J, Pérez-Juste J, Mulvaney P, Liz-Marzán L. Spatially-directed oxidation of gold nanoparticles by Au(III)–CTAB complexes. J Phys Chem B. 2005;109(30):14257–61.
24. Hoffman DR, Aalseth BL, Campbell DH. The use of Freund's complete adjuvant in producing anti-hapten antibody. Immunochemistry. 1969;6(4):632–4.
25. Nikoobakht B, El-Sayed MA. Preparation and growth mechanism of gold nanorods (NRs) using seed-mediated growth method. Chem Mater. 2003;15(10):1957–62.
26. Orendorff CJ, Murphy CJ. Quantitation of metal content in the silver-assisted growth of gold nanorods. J Phys Chem B. 2006;110(9):3990–4.
27. Rao HH, Xue X, Wang H, Xue ZH. Gold nanorod etching-based multicolorimetric sensors: strategies and applications. J Mater Chem C. 2019;7(16):461–2.
28. Wu L, Li GH, Xu X, Zhu L, Huang RM, Chen XQ. Application of nano-ELISA in food analysis: recent advances and challenges. TrAC Trends Anal Chem. 2019;113:140–56.

Publisher's Note